Monthly Notices
of the
ROYAL ASTRONOMICAL SOCIETY

Mon. Not. R. Astron. Soc. **416,** 2477–2493 (2011) doi:10.1111/j.1365-2966.2011.18599.x

STEREO observations of stars and the search for exoplanets

K. T. Wraight,[1⋆] Glenn J. White,[1,2] D. Bewsher[3] and A. J. Norton[1]

[1]*Department of Physics and Astronomy, The Open University, Milton Keynes MK7 6AA*
[2]*Space Science and Technology Department, STFC Rutherford Appleton Laboratory, Chilton, Didcot, Oxfordshire OX11 0QX*
[3]*Jeremiah Horrocks Institute, University of Central Lancashire, Preston, Lancashire PR1 2HE*

Accepted 2011 February 23. Received 2011 February 23; in original form 2010 December 16

ABSTRACT

The feasibility of using data from the NASA *STEREO* mission for variable star and asteroseismology studies has been examined. A data analysis pipeline has been developed that is able to apply selected algorithms to the entire data base of nearly a million stars to search for signs of variability. An analysis limited to stars of magnitude 10.5 has been carried out, which has resulted in the extraction of 263 eclipsing binaries (EBs), of which 122 are not recorded as such in the SIMBAD online data base. The characteristics of the *STEREO* observations are shown to be extremely well suited to variable star studies with the ability to provide continuous phase coverage for extended periods as well as repeated visits that allow both short- and long-term variability to be observed. This will greatly inform studies of particular stars, such as the precataclysmic variable V471 Tau, as well as the entire classes of stars, including many forms of rotational variability. The high-precision photometry has also revealed a potentially substellar companion to a bright ($R = 7.5$ mag) nearby star (HD 213597), detected with 5σ significance. This would provide a significant contribution to the exoplanet research if follow-up observations ascertain the mass to be within the planetary domain. Some particularly unusual EBs from the recovered sample are discussed, including a possible reclassification of a well-known star as an EB rather than a rotational variable (HR 7355) and several particularly eccentric systems, including very long period EBs.

Key words: methods: data analysis – space vehicles: instruments – binaries: eclipsing – stars: individual: HD 213597 – stars: individual: NSV 7359 – stars: individual: V471 Tau.

1 INTRODUCTION

The *STEREO* mission consists of two satellites in heliocentric orbit, each observing the solar environment from the Sun's atmosphere out to the Earth's orbit and together producing 3D images of this region (Kaiser et al. 2008). The Heliospheric Imager (HI-1) onboard the *STEREO*-Ahead spacecraft (HI-1A) has been used to conduct a survey for the variability of stars down to magnitude 12 in its field of view (within about 20° of the ecliptic plane, see Fig. 1). The light curves produced have been analysed to look for exoplanet transits and eclipsing binaries (EBs). The values of eclipsing variables in studies of stellar properties and evolution are well known (de Mink, Langer & Izzard 2011) and the trends from this sample, as well as some particular stars of interest, will prove informative. The detection of many new EBs around comparatively bright stars, previously undetected in many cases due to shallow eclipses, allows for the detailed follow-up required to improve upon existing models of stellar evolution and behaviour. Also of note is a comparison of the effectiveness of different algorithms in extracting the signatures of EBs of different types.

The rest of this paper is divided into sections giving an overview of the *STEREO*/HI-1A characteristics and describing the data analysis pipeline, the results obtained, prospects for further study and the conclusions that can be drawn, and the table showing all 263 EBs is given in the Supporting Information.

Further research is being undertaken to identify and characterize other kinds of variability, which will be the subject of future papers. Some HI-1B data have been extracted (for a region between 50° and 60° right ascension and 10° and 20° declination, which includes a variety of interesting objects e.g. V 471 Tau – see Section 4), but these have not yet been analysed on a large scale. The HI-1B imager is on the side of the spacecraft facing the direction of travel and the light curves show artefacts resulting from micrometeorite impacts, complicating the task of signal extraction.

2 *STEREO*/HI-1A INSTRUMENTATION AND DATA PREPARATION

The HI-1 onboard the HI-1A provided the data for the large-scale analysis. A summary of the data analysis pipeline is given in Appendix A. This instrument is described in detail in Eyles et al. (2009) but for convenience a summary is given here. The HI-1A has a field

⋆E-mail: k.t.wraight@open.ac.uk

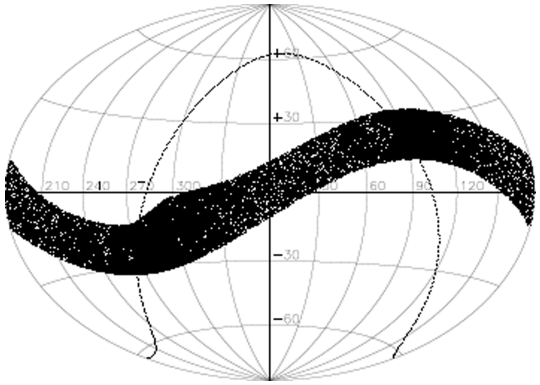

Figure 1. The locations of stars in the *STEREO*/HI-1A with the measured mean magnitude of 9th magnitude and brighter.

of view of 20° × 20° and is centred at a point 14° away from the centre of the Sun, where the solar F-corona is the dominant large-scale structure. The aperture of the HI-1A lens system is 16 mm, with a focal length of 78 mm. The CCD has a pixel size such that the plate scale becomes 35 arcsec on a 2048 × 2048 chip, with images binned 2 × 2 onboard, resulting in 1024 × 1024 images being returned with an image bin size of 70 arcsec. A filter limits the spectral bandpass to 630–730 nm with some contribution around 400 and 950 nm. The characteristics of the CCD on the HI-1B are similar, with only slight differences in the spectral bandpass (Eyles et al. 2009). Each image is the result of 30 summed exposures, each of 40 s, with one image produced every 40 min. This prevents saturation by cosmic rays, although planetary and cometary incursions do cause saturation, and also allows for very faint structures in coronal mass ejections and the solar environment to be detected. Stars down to 12th magnitude are detectable and about 650 000 stars have been recorded with listed magnitudes brighter than 11.5, with almost 75 000 of these being brighter than magnitude 9.5 (Fig. 1). Only the very brightest stars, those brighter than about 3rd magnitude, saturate the detector but useful light curves can nevertheless still be extracted. Since these stars are mostly within 20° of the ecliptic plane, the *STEREO*/HI-1A and HI-1B are therefore searching for a region of the sky not well observed by dedicated exoplanet searches, such as *CoRoT* (Auvergne et al. 2009) (*V* magnitudes from 11 to 16), *Kepler* (Koch et al. 2010) (*R* magnitudes from 7 to 17) and SuperWASP (Pollacco et al. 2006) (*V* magnitudes from 9 to 13), and they are also able to view much brighter stars than are normally observed.

Before the data from the *STEREO*/HI-1A and HI-1B can be analysed, it must be passed through a pipeline (shown in Appendix A, Fig. A1) in order to

(i) make a shutterless correction (Eyles et al. 2009);
(ii) apply a large-scale flat-field (Bewsher et al. 2010);
(iii) apply the pointing calibration to determine the positions of stars (Brown, Bewsher & Eyles 2009);
(iv) flag out saturated pixels/columns and missing data blocks (Eyles et al. 2009); and
(v) carry out a daily background subtraction.

2.1 Shutterless correction

The *STEREO*/HI-1A and HI-1B cameras have no shutter and remain exposed during the readout process and also during the clear process prior to each exposure. Consequently, the top of the image is exposed for longer than the bottom of the image, resulting in

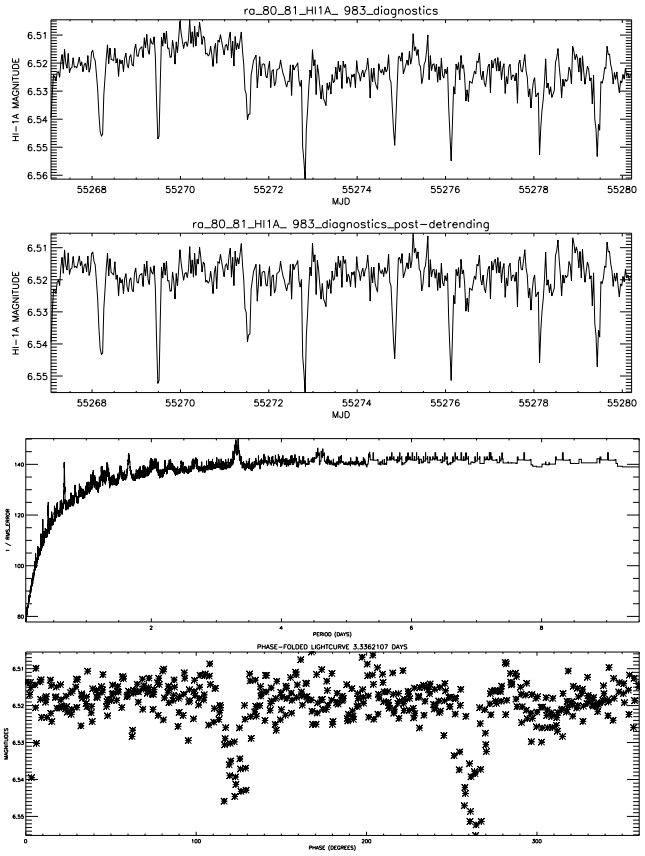

Figure 2. The main stages of the detrending and analysis, demonstrated by the star HR 1750. Starting from the top panel showing the raw light curve for one epoch of observations, the second panel shows the results of detrending with a seventh-order polynomial, the third panel shows the periodogram derived from the detrended light curve and the bottom panel shows the light curve phase-folded on the period of the strongest signal found from the periodogram. Note that it is unknown whether the trend removed by the polynomial fitting is artificial or genuine variability – this potential long-term variability is not the type of variability being searched for.

image smearing during readout. The effect of this can be expressed as a matrix relationship and a correction for the effects of the shutterless operation can be made by a matrix multiplication. If saturation occurs anywhere in a column, then the signal in the affected pixels cannot be corrected in this way and the entire column is flagged as bad data. Further details can be found in Eyles et al. (2009).

2.2 Flat-fields

The sensitivity of the *STEREO*/HI-1A and HI-1B cameras varies spatially in three distinct ways. First, the optical properties mean that the solid angle corresponding to each pixel may vary across the field of view, leading to large variations in the scale across the CCD. Secondly, the sensitivity of the CCD varies for individual pixels, independently of the sensitivity of adjacent pixels. Thirdly, debris and manufacturing variations and defects on the CCD generate variations in sensitivity over the scale of tens to hundreds of pixels.

It is unknown to what extent the sensitivity of the CCD will vary over time but it is anticipated that the largely stationary F-corona in the field of view may be enough to cause some degradation. The flat-field calibration is updated on a regular basis, however, which should prevent this becoming a problem.

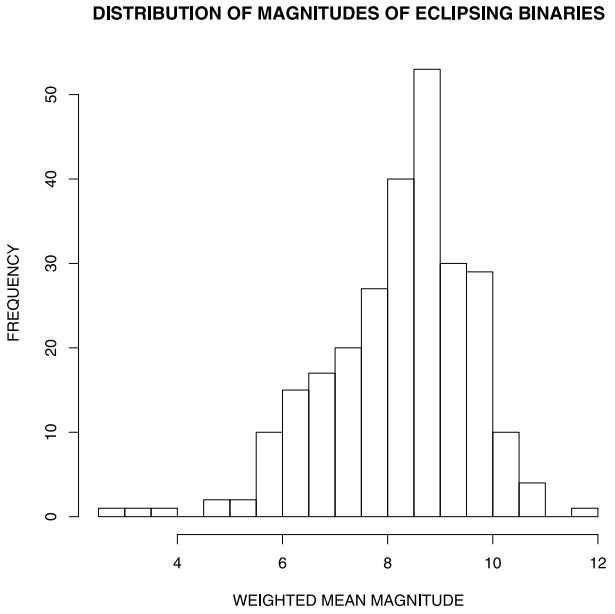

Figure 3. The distribution of the 263 EBs observed by the *STEREO*/HI-1A by the weighted mean magnitude. The fall-off after magnitude 9 is the result of the decreasing signal quality with the magnitude increasingly preventing the detection of eclipse signatures.

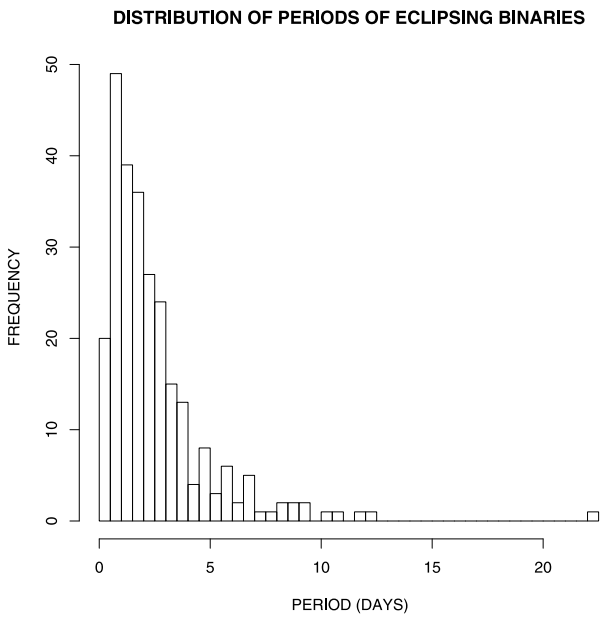

Figure 4. The distribution of the 263 EBs observed by the *STEREO*/HI-1A by period.

The flat-field calibrations are performed on *STEREO*/HI-1A and HI-1B images after the removal of the CCD DC bias (Eyles et al. 2009) and the application of the shutterless correction.

Images with significant optical ghosts due to saturated objects in the data are not used for flat-fielding. The methodology is given in full in Bewsher et al. (2010). Observations of stars near a region of the frame close to the edge of the solar disc are discarded due to additional noise of solar origin.

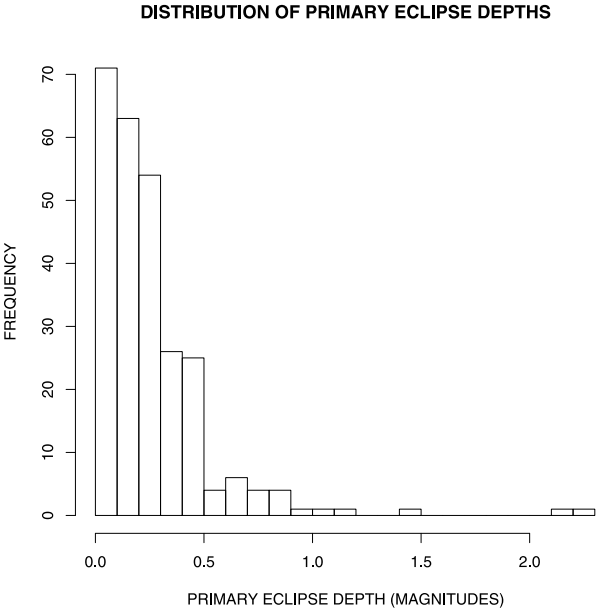

Figure 5. The distribution of the 263 EBs observed by the *STEREO*/HI-1A by primary eclipse depth.

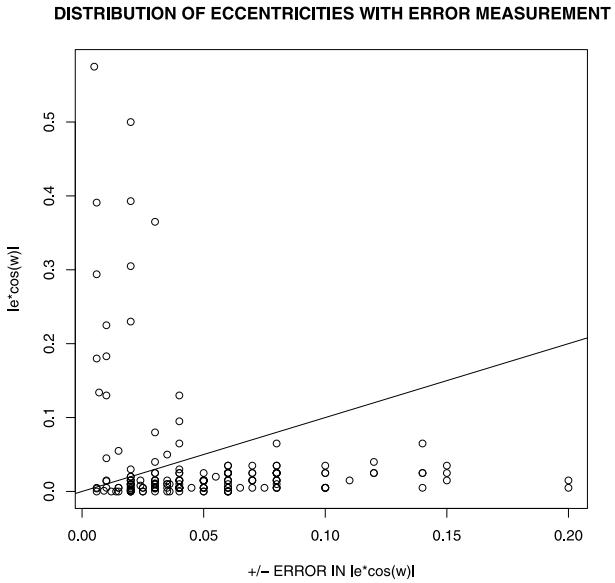

Figure 6. The estimates of the minimum eccentricities ($|e \times \cos\omega|$) of the 263 EBs observed by the *STEREO*/HI-1A, where measurable, against the errors for each measurement. Each open circle represents a single EB. Those points above the line represent EBs for which an eccentricity of zero is outside the range of the errors in the measurement.

2.3 Pointing calibration

Calibrated instrument pointing solutions have been derived by comparing the locations of stars identified in the *STEREO*/HI-1A and HI-1B images with known star positions given in the NOMAD astrometric data set (Zacharias et al. 2004). In the raw (L0.5) data, nominal pointing information is provided; however, once the data have been processed to L1 (by running secchi_prep), the calibrated pointing information is provided. A complete description on the calibration and pointing procedure can be found in Brown et al. (2009).

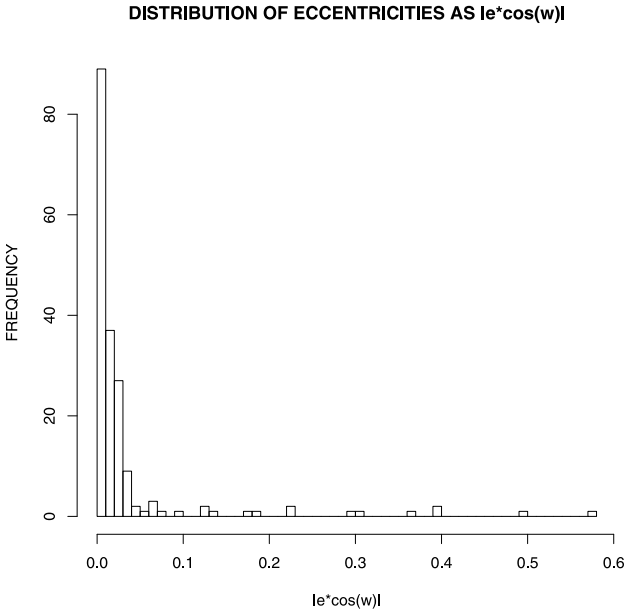

Figure 7. The estimates of the minimum eccentricities ($|e \times \cos\omega|$) of the 263 EBs observed by the *STEREO*/HI-1A, where measurable.

For the *STEREO*/HI-1A and HI-1B cameras, the average root-mean-square distance between stars as seen in the image and the location given in the catalogue is about 0.1 pixels, that is, 7 arcsec. Thus, any pointing offsets have a negligible effect on the efficacy of the stellar light curves.

2.4 Photometric calibration

The methodology used to determine the photometric calibration is described in full in Bewsher et al. (2010), which includes more up-to-date flat-fields and calibration constants than were available for the analysis presented in this paper. Aperture photometry of well-isolated stars down to 12th magnitude is used that have no other stars with a difference of $\leq$1 mag within 1000 arcsec.

Whilst future large-scale analyses will use the most up-to-date calibration of Bewsher et al. (2010), the photometric calibration of the *STEREO*/HI-1A used in the analysis presented herein is described by the following formula:

$$\textit{STEREO}\ \text{magnitude} = d \log\left(\frac{\text{counts}}{c}\right), \quad (1)$$

where $d = -2.495\,01$ and $c = 18\,337.7$ for the *STEREO*/HI-1A for a 3.5-pixel-radius aperture. The number of counts is expressed as a flux intensity in units in data numbers, DN s^{-1}, as provided by secchi_prep. For analysing the *STEREO*/HI-1B data, the following formula is used (explained more fully in Bewsher et al. 2010):

$$\textit{STEREO}\ \text{magnitude} = d \log\left(\frac{a \times \text{counts}}{b \times c}\right), \quad (2)$$

where $d = -2.5$, $a = 4$ is a correction factor, and $b = 0.98$ and $c = 97\,026$ are the calibration constants for the *STEREO*/HI-1B for a 3.5-pixel-radius aperture.

3 DATA ANALYSIS PIPELINE AND METHODS

Three methods were used to quantify the variability of each star in the *STEREO*/HI-1A data base with a magnitude of 10.5 or greater, thus eliminating the faintest stars with the lowest signal-to-noise ratio. (Fig. 1 shows the locations of stars with the measured mean magnitude of 9th magnitude and brighter with more than 20 photometric points on their light curves.) They were the box-least-squares (BLS) (Kovács, Zucker & Mazeh 2002), the Lomb–Scargle periodogram (Scargle 1982) and Stetson's variability index (Welch & Stetson 1993). The IDL code to produce a Lomb–Scargle periodogram was obtained from the Armagh Observatory, whilst the others were custom implementations. Fig. 2 shows the steps in the analysis as produced by the programs doing the analysis.

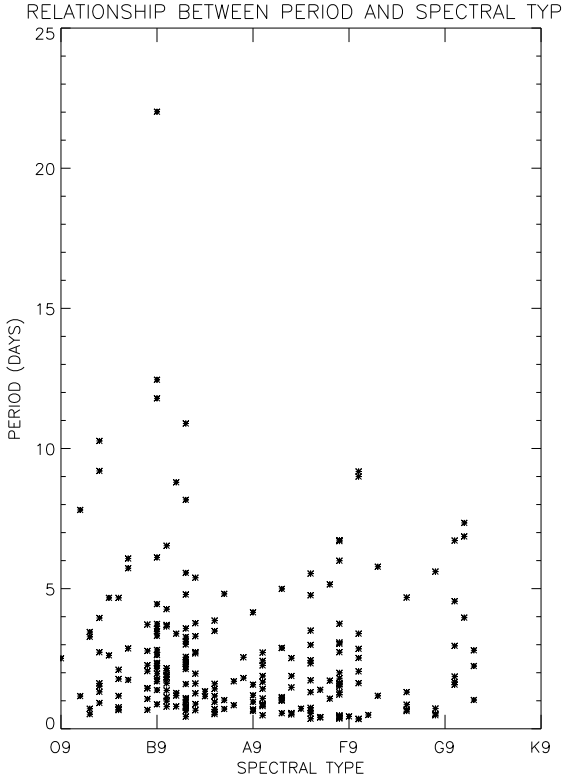

Figure 8. The 232 EBs observed by the *STEREO*/HI-1A with a known spectral type, showing the relationship between the spectral type and period. The most common spectral type is A2, with 22 stars in the sample. There are no clear patterns connecting the spectral type with the period; however, there are some cases where the specific star causing the eclipses has not been identified and the spectral type is of the star closest to the target coordinates (see Appendix A).

Before being passed to the algorithms for analysis, a seventh-order polynomial fit was carried out for each light curve to remove both natural and artificial trends that might obscure the faintest transit signals (the top two panels of Fig. 2 show an example light curve before and after this polynomial detrending). It should be emphasized that whether or not there is genuine long-term variability that would be removed by this is not a concern as the focus is on recovering eclipsing variables and exoplanet transits whilst retaining the capacity to detect other short-term variables, such as RR Lyrae and δ Scuti stars. The IDL built-in routine poly_fit was the basis of this. Each light curve was then passed through a combined low- and high-pass filter in an attempt to remove some remaining noise. This was done by transforming into the frequency domain using the IDL built-in routine fft and applying a mask that blocked all features within one standard deviation of the mean before using the inverse transform to return to the time-domain. This process was repeated for each epoch of observations for each star and each epoch was analysed separately by the different algorithms. (The third panel

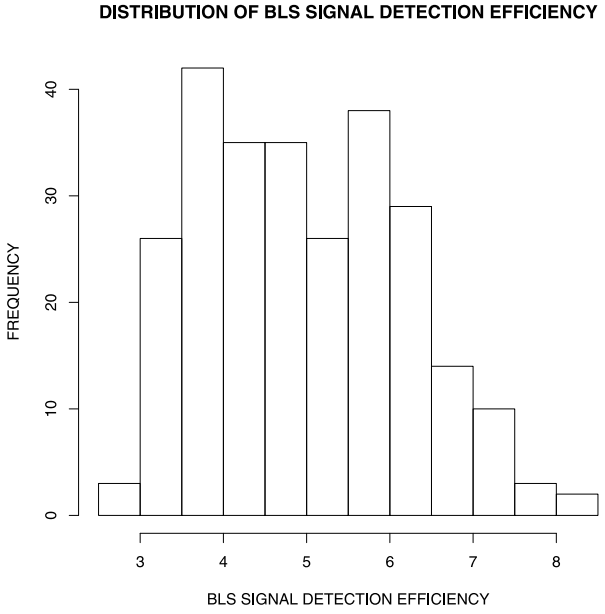

Figure 9. The distribution of the 263 EBs observed by the *STEREO*/HI-1A by BLS SDE.

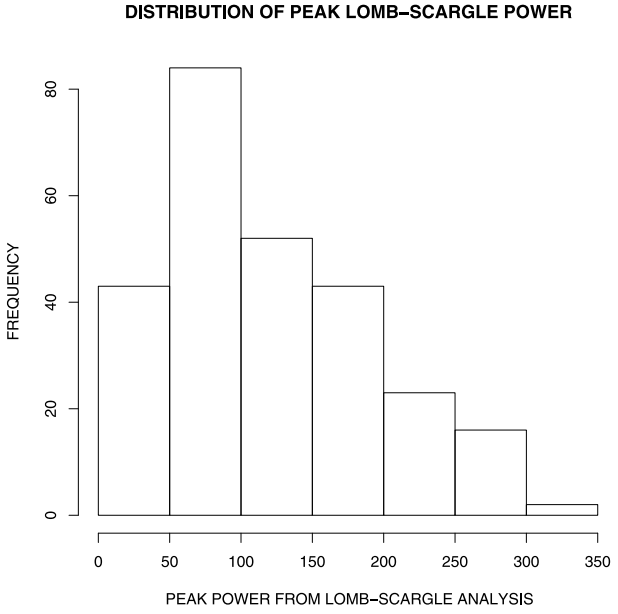

Figure 10. The distribution of the 263 EBs observed by the *STEREO*/HI-1A by peak power from a Lomb–Scargle periodogram analysis.

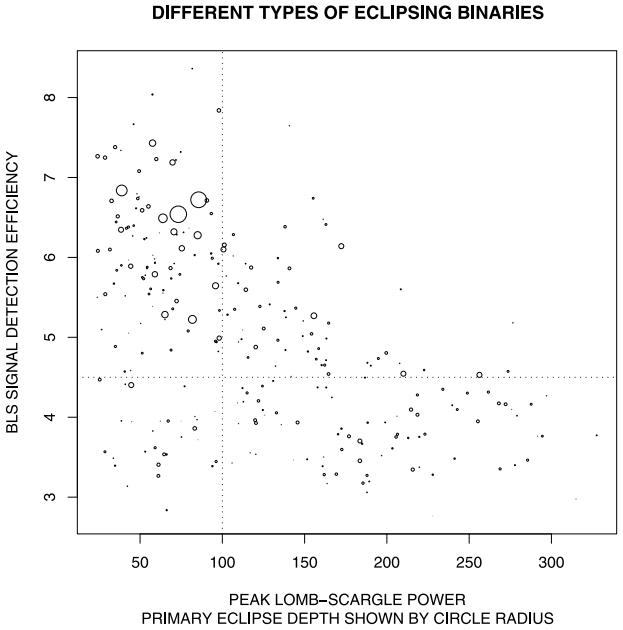

Figure 11. Comparison of the ability of the BLS and Lomb–Scargle algorithms to extract the signals of EBs. Each EB is represented by a circle with a radius proportional to the depth of the primary eclipse. The points above the horizontal line have a SDE high enough to be considered a detection by the BLS algorithm, whilst those to the right-hand side of the vertical line may similarly be considered to have been detected by the Lomb–Scargle algorithm, in the absence of artefacts and noise producing large numbers of similar signals. Those rated poorly by both were typically found through visual examination.

from the top in Fig. 2 shows the BLS spectrum.) The strongest signals found from analysing all the epochs for each star were recorded and stored in an output file associated with each field of view, as were a variety of other statistics (see the Appendices).

The reasons for processing each epoch separately are the presence of noise and artefact features that exist within one or more epochs, but seldom all, such as a planetary incursion into the field of view by Venus or Mercury, the existence of some features near the beginning or end of some epochs as a result of streamers or other solar activity and the presence of occasional depointing events, typically from micrometeorite impacts, all of which would produce a false signal if all epochs were analysed together. As the highest values from all epochs are stored, these features still give some false signals but by analysing data from unaffected epochs a genuine value may sometimes supersede the false one. Nevertheless, the severity of some noise and artefacts precludes the detection of faint signals, which is only partially alleviated in some cases by a direct visual inspection of light curves for signs of genuine variability.

Once a star had been identified as an EB candidate on the basis of the statistics generated, its detrended, filtered light curve and phase-folded light curves on the periods of the strongest signals found by the BLS and Lomb–Scargle analysis were examined visually to determine if the variability detected was likely to be genuine. An initial classification of the type of variability was made at this stage. Those that were considered likely to be EBs were imported into the software package PERANSO (Vanmunster 2008) for more detailed analysis. There is the possibility that many contact binary systems might have been excluded at this stage due to an inability to distinguish between different types of variability. Indeed, there is some evidence that a significant number of fainter contact binaries may have been excluded in this manner (Section 6).

Within PERANSO, a detailed analysis of the BLS spectrum would be used to establish as accurate a period as possible using as many epochs as possible, using the software's ability to manually exclude observation points that are likely to be noise or artefacts. The light curve phase-folded from this period would be used to finally determine if the star was likely to be an EB. If it was still considered an EB, the phase-folded light curve would provide estimates of the primary eclipse depth and minimum eccentricity. The minimum eccentricity would be estimated by visually determining the offset of secondary eclipses, where these could be distinguished as such, from a phase of 0.5 away from the primary eclipse. The estimated errors in the estimate were taken as the extremes of the possible

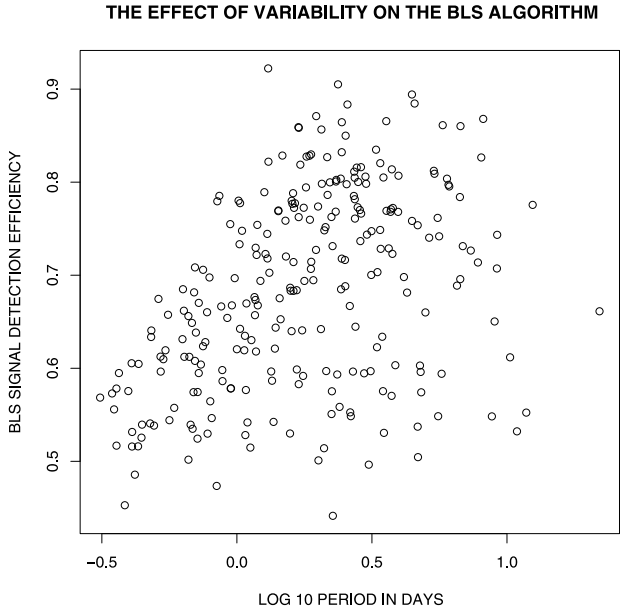

Figure 12. The dependence of the BLS algorithm on the period of a signal. The influence is believed to be the shape of the light curves of variables with increasingly short periods, rather than the period itself. Each open circle represents a single EB.

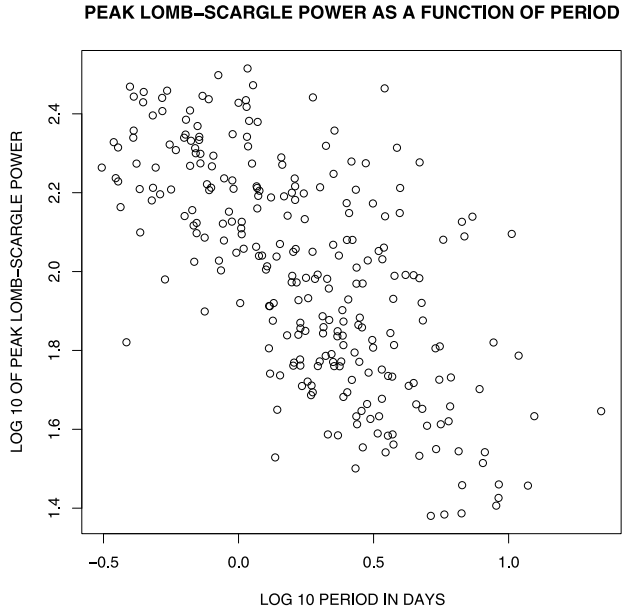

Figure 13. The dependence of the Lomb–Scargle method on the period of a signal. Each open circle represents a single EB.

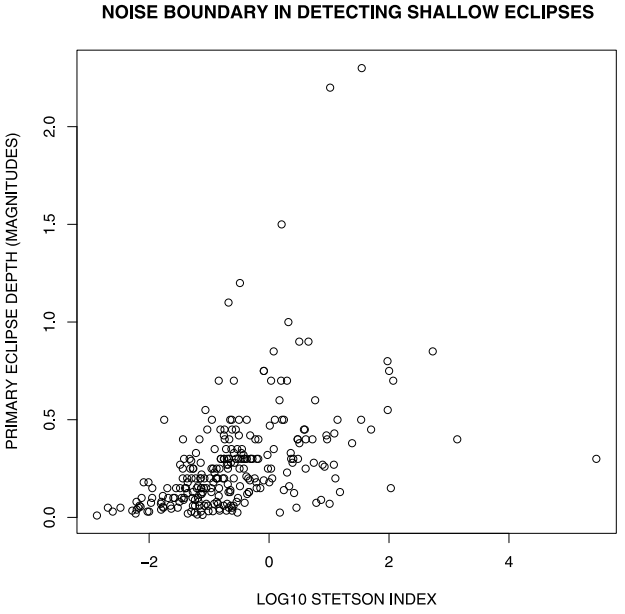

Figure 14. The dependence of the primary eclipse depth on the Stetson index. The sharp cut-off at about −0.5 shows that eclipses with a primary eclipse depth less than 0.3 mag are considerably more difficult to detect through noise or variability. Each open circle represents a single EB.

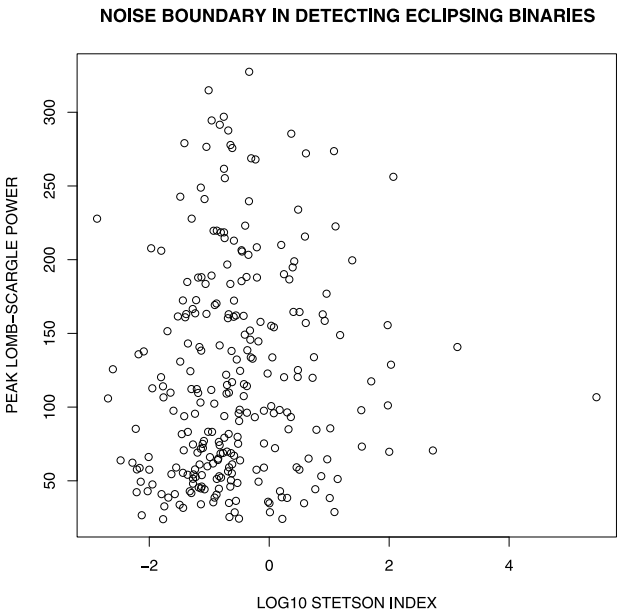

Figure 15. The dependence of the peak power from a Lomb–Scargle periodogram analysis as a function of the Stetson index. The cut-off point at about −0.5 shows that variability or noise above a certain level is very effective at obscuring the signals of EBs, regardless of their peak power. Each open circle represents a single EB.

ranges of where the secondary minimum might be; thus, the errors are larger for smoother, shallower eclipses as in many contact binaries. The values obtained were then, along with the errors, multiplied by 2, giving a value that is actually $|e \times \cos \omega|$ or effectively a minimum eccentricity that could be significantly higher depending on the value of ω, the argument of periastron.

The values of the period, primary eclipse depth and $|e \times \cos \omega|$ found from this detailed examination were recorded, along with the output of the different algorithms, the star's celestial coordinates, its identity (from the SIMBAD) and spectral type (from the SIMBAD) as well as the identity of any nearby star (within 6 arcmin, from the SIMBAD) that could potentially have contaminated the signal and whether or not either the star or this neighbour had previously been identified as an EB. This data set of 263 EBs (Table A1) was then explored for interesting trends and patterns.

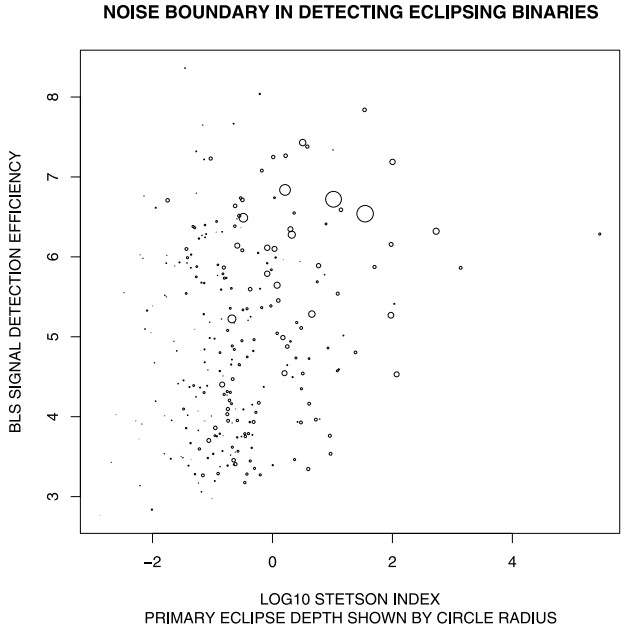

Figure 16. The dependence of the SDE as a function of the Stetson index. The cut-off point at about −0.5 shows that variability or noise above a certain level is obscuring the signals of some EBs, although the apparent clustering of signals around a moderate value and especially the higher ratings for deeper eclipses show that the Stetson index is also to some extent reflecting the variability due to eclipses. Each EB is represented by a circle with a radius proportional to the depth of the primary eclipse.

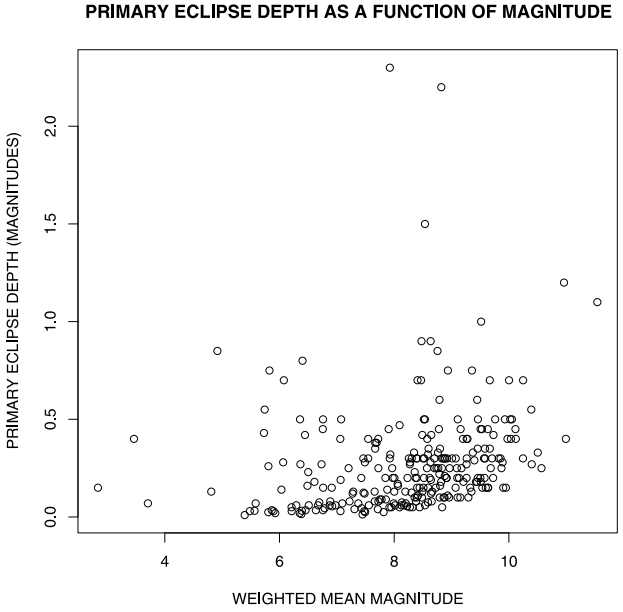

Figure 17. The dependence of the primary eclipse depth as a function of the weighted mean magnitude. After about magnitude 8.5, shallower eclipses are not detected, with the threshold rising nearly linearly. Each open circle represents a single EB.

3.1 Trends

The distributions of the recorded characteristics show some trends that apply to the sample as a whole. Most significantly, the distribution of EBs by the weighted mean magnitude (Fig. 3) shows a peak between magnitude 8.5 and 9.0 after which the numbers extracted fall off. This implies that, due to a combination of sensitivity and noise, eclipses are not being detected around fainter stars since the distribution of EBs is expected to match the distribution of stars in the data base, the numbers of which continue to increase with increasing magnitude.

The periods given in the statistics are the primary-to-primary period, although the difficulty in distinguishing primary from secondary eclipses may cause the resulting value to be out by a factor of 2. The distribution of the periods of the EBs extracted reflects, as expected, the bias due to the length of individual epochs (Fig. 4). In order to get a good signal, three transits must be observed within an epoch and thus there is a tendency to find periods of less than this threshold. Through the presence of secondary eclipses, longer periods can be found but visual examination is required for detecting the very longest period EBs, especially if the system is eccentric. The star with the longest period confirmed of the 263 is HD 72208 with 22.013 d (see Section 4 for details), which cannot be found through a separate analysis of each epoch but only through all three epochs presently available, owing to the significant eccentricity ($|e \times \cos\omega| = 0.391 \pm 0.006$) and the fact that no more than two transits are observed in any epoch. There is a suspected EB with a potentially longer period, showing only one primary eclipse in each epoch (HD 173770, see Section 4), but a definite period determination cannot be made and it was not included in the sample.

The distribution of the depths of primary eclipses reveals a trend that is interpreted as the presence of different populations of EBs (Fig. 5). Only detached and semidetached EBs appear to have a primary eclipse depth greater than 0.5 mag, whereas contact binaries predominate at depths of 0.3 mag and below.

The estimates of $|e \times \cos\omega|$ reveal that 24 out of the 263 EBs have measurable eccentricity (Fig. 6) (see Appendix A for their phase-folded light curves). Other EBs in the sample may have eccentricity, as the value of the argument of periastron, ω, is unknown and there are some that show a hint of eccentricity but the margin of error does not preclude the possibility that they might have zero eccentricity, including a couple that are exactly on the line where the error margin equals the estimate of $|e \times \cos\omega|$. Thus, a small but significant fraction of the sample are eccentric, with more than 5 per cent showing significant eccentricity (Fig. 7). The sample of eccentric systems is not quite large enough to show statistically valid trends, unfortunately, although the indications are that small eccentricities dominate with larger eccentricities being widely distributed. Nevertheless, this result is broadly in agreement with recent findings from the *Kepler* mission (Prša et al. 2011); however, the sample of stars observed by the *STEREO*/HI-1A is not limited to main-sequence stars or by other selection criteria intended to maximize the chances of finding an exoplanet transit. It is therefore useful to find a similar distribution of $|e \times \cos\omega|$ to the *Kepler* sample as it implies that eccentricity is not dependent on the spectral type. Eccentric systems are expected to circularize over time and thus these systems are much studied in the field of stellar evolution to model interactions between multiple stars as an interaction with a third body is usually required for them to be formed (Claret & Willems 2002).

The distribution of spectral types of the EB primary stars shows a predominance of younger, hotter stars of earlier spectral types (Fig. 8). The main limitation of this distribution is that the spectral type of the closest star to the coordinates of the perceived EB may not always be the star that is actually eclipsing, due to the low spatial resolution and the possible contamination of light curves by nearby stars. The distribution will also be affected by any bias in the

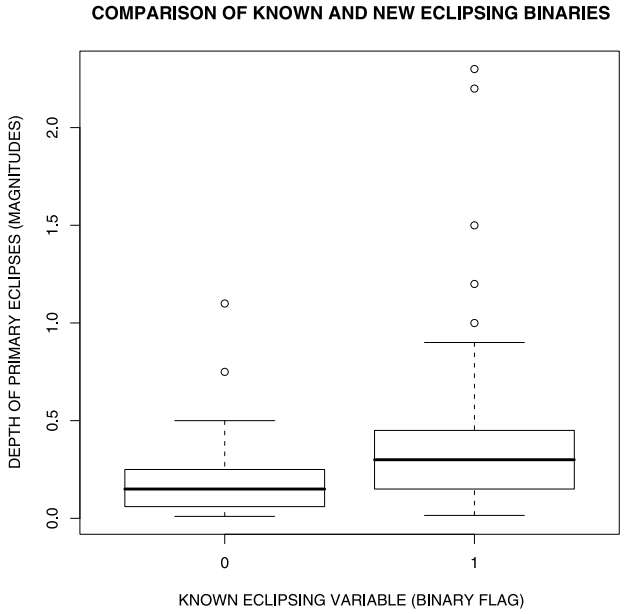

Figure 18. Comparison of the distribution of known and new EBs with respect to the depth of their primary eclipses. The tendency of the newly discovered systems to show fainter eclipses reflects both the sensitivity of the *STEREO*/HI-1A and the expected bias of previous surveys in discovering deeper eclipses. The centre box contains those EBs in the second and third quartiles with the median represented by a thick line within, whilst the outer bars represent an approximately 95 per cent confidence level and outliers are individual open circles.

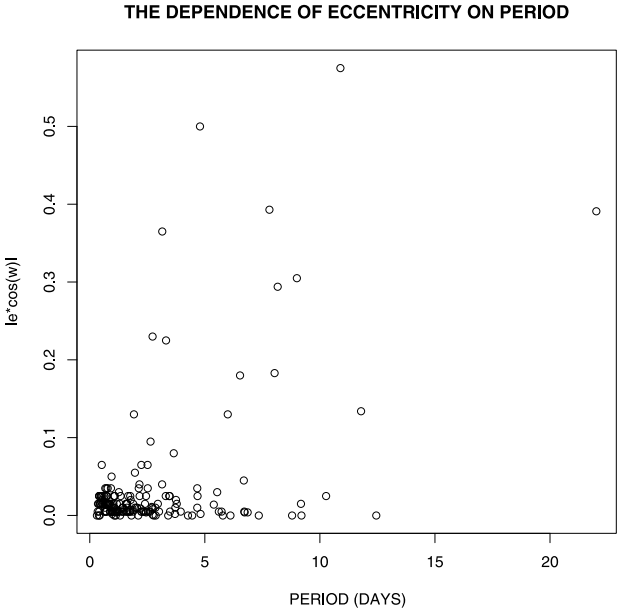

Figure 19. The dependence of the minimum eccentricity of the 263 EBs observed by the *STEREO*/HI-1A, as measured by $|e \times \cos\omega|$, on the period of eclipses. Each open circle represents a single EB.

STEREO/HI-1A data base, with only stars brighter than magnitude 10.5 being analysed en masse (although one or two fainter examples were identified visually).

The distribution of EBs by their signal detection efficiency (SDE) from the BLS algorithm (Fig. 9) shows two indistinct peaks, interpreted as corresponding to two different types of EBs. The peak with the highest SDE corresponds mostly to detached binaries, whose light curves are a closer match to the box-like shape the BLS algorithm checks for. The broader peak with the lower SDE corresponds to contact binaries, which have smoother, more sinusoidal light curves. An Algol-type binary might be the highest rated by the BLS algorithm in its field, but contact binaries can sometimes be near the bottom of such a list and thus are not reliably detected by this algorithm. The Lomb–Scargle periodogram (distribution shown in Fig. 10) preferentially reveals contact binaries, although it typically does give a signal for many detached binaries as well, albeit increasingly less so for shallower, more-box-like eclipses (Fig. 11). Combining the BLS and the Lomb–Scargle methods thus produces a positive signal for the vast majority of the EBs, with those rated poorly, by both, being stars with fewer data points (both algorithms give higher scores for more data points; thus, stars with less data available are rated less highly), those with very long periods and those with comparatively low signal-to-noise ratio that were detected by visual examination.

The effect of the period on the output of the BLS and Lomb–Scargle methods was also investigated (Figs 12 and 13). The dependence discovered is again likely representative of the shape of the transits.

As a variety of noise signatures were encountered in the data set, some very clearly obscuring genuine signals, producing both false positives and false negatives, an attempt to evaluate the effects of noise was made (Figs 14–17). Together these appear to show a tendency to overlook shallow eclipses. This may be partly due to a mixture of red and white noise and also due to problems classifying contact binaries as such when their light curves are not clear enough to distinguish them from sinusoidal variations. Blending also has a tendency to obscure faint signals, with the brightest object in the photometric aperture dominating but showing additional signals overlaid or with stars of similar magnitudes showing constructive or destructive interference resembling an amplitude modulation. This has the effect of lowering, broadening and sometimes splitting peaks in a periodogram analysis, which affects the ability of an algorithm to identify a low-amplitude signal.

Since a large proportion of the sample of EBs appear to be previously undetected or, at least, unconfirmed as such by previous observations, a search was made for characteristics in common to understand what, if anything, might be different about the new cases that might explain why they had previously gone undetected (Fig. 18). As might be expected, there is a tendency for the new cases to have shallower eclipses than those previously known. There does not appear to be any significant difference in either the periods or the magnitudes found, however.

A previously known tendency for EBs with long periods to be more likely to be eccentric (Mathieu & Mazeh 1988) is confirmed by the *STEREO*/HI-1A observations (Fig. 19).

To summarize briefly, the BLS is the algorithm of choice for extracting box-like eclipses, for example, Algol binaries or exoplanet transits. The Lomb–Scargle algorithm is best at extracting sinusoidal-like signals but also has some limited capability to extract other regular signals. The Stetson index is able to extract large-amplitude variables of all types.

4 RESULTS

Of the 263 EBs extracted, 122 are not recorded as such in the SIMBAD. Some of these are, however, known variables of other types or are suspected of variability. Owing to the purely

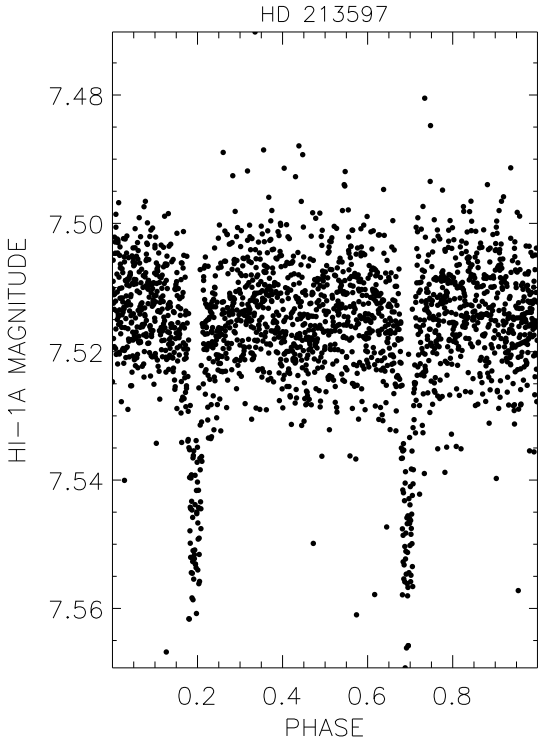

Figure 20. Light curve of the star HD 213597, phase-folded on a period of 4.8476 d.

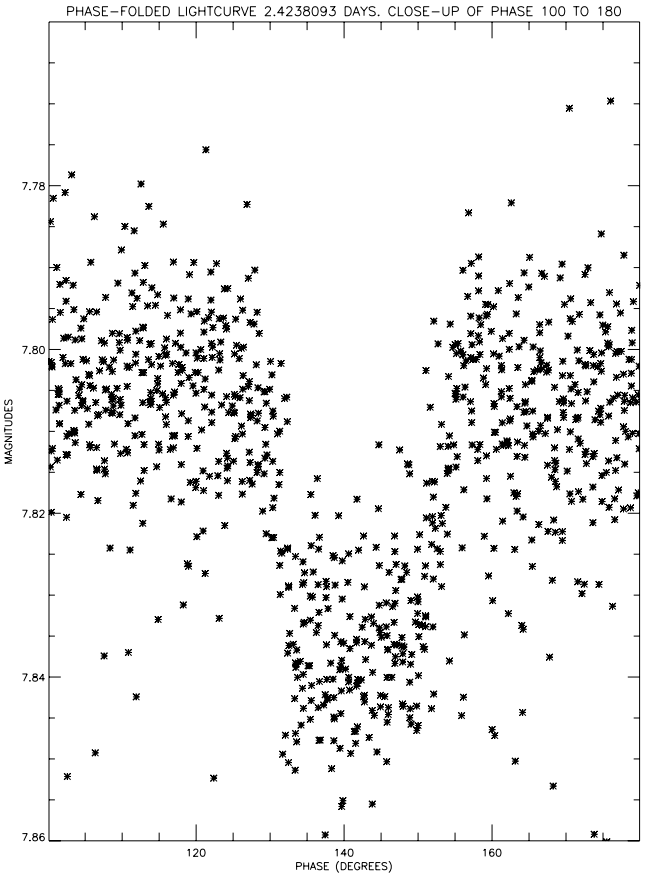

Figure 21. Close-up of the transit of HD 213597, phase-folded on a period of 2.4238 d. This light curve was constructed using the latest data available, including updated flat-fields as well as data from the *STEREO*/HI-1B.

photometric data available from the *STEREO*/HI-1A, there remains the possibility of misclassification; however, care was taken to include only stars whose phase-folded light curves appeared to be clear cases. Thanks to the excellent phase coverage resulting from the *STEREO*/HI-1A observational cadence of 40 min maintained for up to 19.44 d, with three or four such epochs for most stars, the new observations are in many cases clearer than those previously available and in some cases the existing classification may be in need of revision. A total of 24 of the EBs have measurable eccentricity and their light curves are shown in Appendix A (Fig. A2).

4.1 Individual stars of interest

4.1.1 HD 213597: substellar transit candidate

The best potentially substellar transiting candidate is HD 213597. This star is recorded in the SIMBAD as being of spectral type F0 and is not suspected of any variability. The observed eclipses are box like, with very sudden ingress and egress phases, and are uniformly about 25 mmag deep, with a period of 2.4238 d between successive eclipses (Figs 20 and 21). Secondary eclipses are not evident.

4.1.2 V471 Tau: cataclysmic variable progenitor

Although it does not feature in the sample, as the eclipses by the white dwarf secondary are too short to be observed, V471 Tau nevertheless is an important star and the *STEREO* observations in both the HI-1A (Fig. 22) and the HI-1B (Fig. 23) have the potential to inform studies of the magnetic activity cycle of the red dwarf primary (e.g. O'Brien, Bond & Sion 2001; Hussain et al. 2006; Kamiński et al. 2007). As a cataclysmic variable progenitor, with an unexpectedly massive red dwarf primary and the most massive white dwarf in the Hyades (O'Brien et al. 2001), studies of this star may have a considerable effect on understanding the mechanism behind Type 1a supernovae, thereby influencing the calibration of the extragalactic distance scale and much of modern cosmology. Note that the spectral bandpass of the HI-1A and HI-1B imagers allows a component of blue light through (Bewsher et al. 2010) and the white dwarf secondary is estimated to contribute 6 per cent of the flux in this part of the spectrum (O'Brien et al. 2001). Similar behaviour can be seen in *STEREO* observations of RS CVn variables, for example, SZ Psc, and shows that the *STEREO* is a useful resource for studies of similar variability that require photometry with both long and short baselines.

4.1.3 Highly eccentric EBs

The most eccentric undiscovered EB in the sample is HIP 92307, with $|e \times \cos\omega| = 0.500 \pm 0.020$ (Fig. 24). Both primary and secondary eclipses are about 30 mmag deep; indeed, it is not clear which are the primary and which are the secondary eclipses. This star is listed as spectral type A2V.

The longest period EB in the sample is HD 72208, with 22.0130 d between primary eclipses and $|e \times \cos\omega| = 0.391 \pm 0.006$, making it one of the more eccentric as well (Fig. 25). This star, spectral type B9p, is a spectroscopic binary. Both primary and secondary eclipses are about 60 mmag deep.

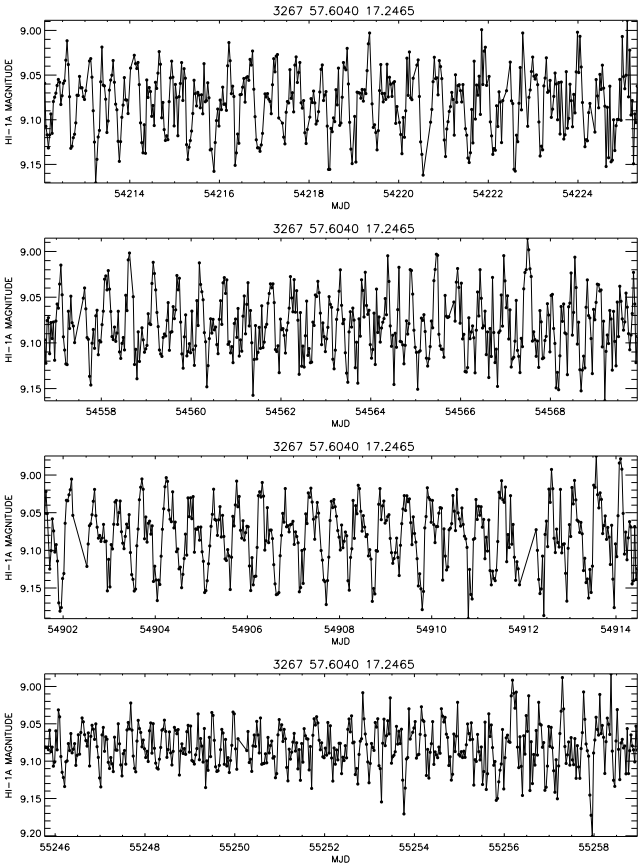

Figure 22. Light curve of the star V471 Tau, as observed by the *STEREO*/HI-1A. 3267 is the catalogue number of the star in the *STEREO* HI-1A field of view for right ascension 50°–60° and declination 10°–20°.

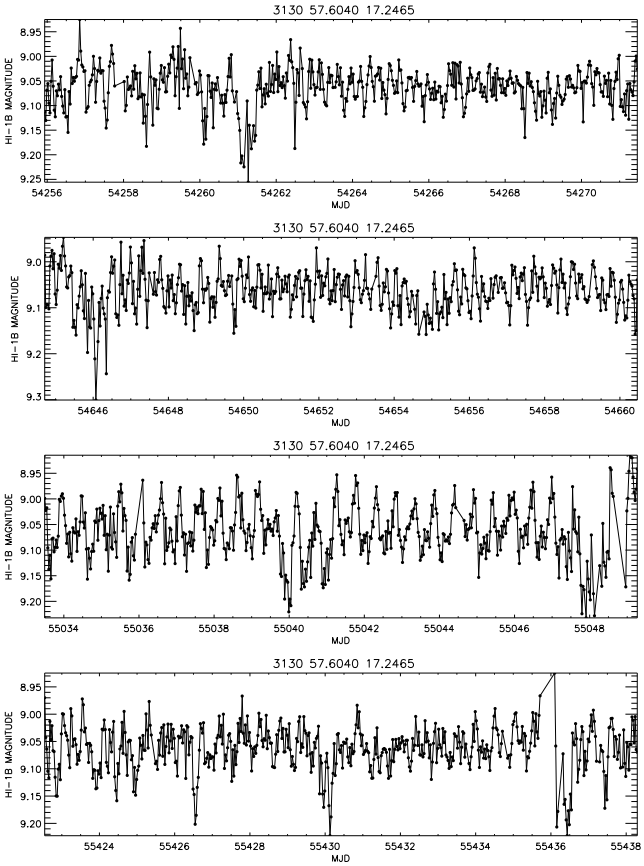

Figure 23. Light curve of the star V471 Tau, as observed by the *STEREO* HI-1B imager. 3130 is the catalogue number of the star in the *STEREO* HI-1B field of view for right ascension 50°–60° and declination 10°–20°. The scale of the *y*-axis has been adjusted to fit the data range.

Possibly the longest period EB so far observed in the *STEREO*/HI-1A data may be HD 173770. As there are multiple possible periods that can fit the light curve, it was not included in the sample. The best-fitting period that has been found with the data available shows a period of 25.145 d, which implies a minimum eccentricity $|e \times \cos\omega| = 0.108 \pm 0.012$. The star shows some intrinsic regular variability as well, although the exact type has not yet been classified. The host star is listed in the SIMBAD as being of spectral type B6V and is a suspected triple system. With the separation given for these components, it is unlikely that either are responsible for the eclipses and this may instead be a quadruple system. The light curve is included in Fig. A2 for comparison with the other measurably eccentric EBs.

4.1.4 NSV 7359: β Cepheid showing the Kozai effect

A well-observed bright star, NSV 7359 shows relatively deep eclipses with a period of 9.1999 d that have not been recorded in the SIMBAD (Fig. 26). This star is a known β Cepheid, with an amplitude listed as 30 mmag. Given the volume of observations, it is very surprising that this variability has not previously been recorded. It is in a fairly crowded area with many stars close by in the *STEREO*/HI-1A field of view, yet none of these is sufficiently bright to contaminate its light curve to the extent of eclipses as deep as those observed. The eclipses are therefore genuine and should help to further inform the parameters previously determined for this star. Interestingly, this star is also shown in the SIMBAD to be a spectroscopic binary with a period of 0.2872 d, which would mean that the eclipsing companion is a tertiary component and not the secondary. The Kozai effect (Kozai 1962) may have caused the inclination of the system to change so that eclipses are now visible.

4.1.5 HR 7355: rotational variable or contact binary?

One of the better-observed stars in the sample is HR 7355 (a.k.a. HIP 95408 and HD 182180). The *STEREO*/HI-1A shows what appears to be a clear-cut case for an EB as the phase-folding on 0.5214 d indicates in Fig. 27. Other studies have noted this periodicity and associated it with a rotation period, however, rather than attributing it to a secondary companion, even the most recent which shows the variability to be eclipse like (Oksala et al. 2010). We suggest that the photometry from the *STEREO* is enough to warrant a reappraisal of the nature of this system. It has been left in the sample as an EB since from the photometry alone that is what it appears to be. In the wider context, it is clearly an unusual and fascinating, chemically peculiar star that continues to attract further study.

4.2 False positives

A small number of stars showing variability on a similar scale to that expected of an exoplanet or brown dwarf transit could be ruled

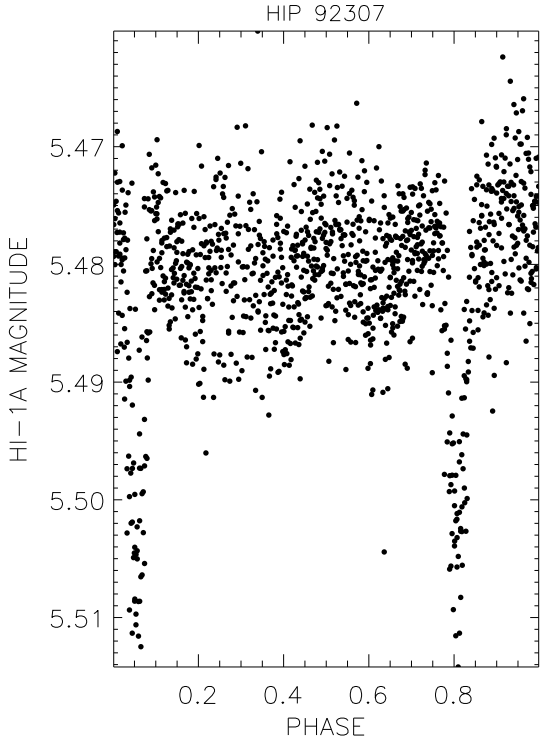

Figure 24. Light curve of the star HIP 92307, phase-folded on a period of 4.7911 d. $|e \times \cos\omega| = 0.500 \pm 0.020$.

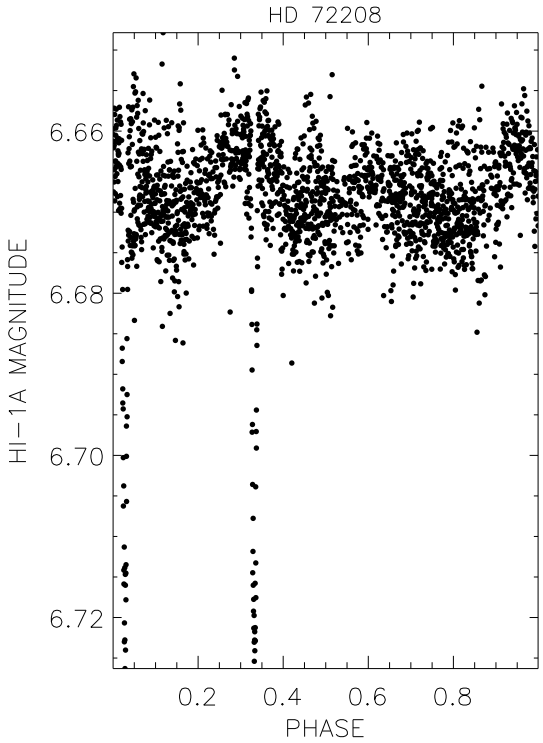

Figure 25. Light curve of the star HD 72208, phase-folded on a period of 22.0130 d. $|e \times \cos\omega| = 0.391 \pm 0.006$.

out as such from photometric data alone, or in combination with other information related to the host star.

Total eclipses just 30 mmag deep were observed around either HIP 248 or HIP 247 (near-identical signals and in the same or adjacent pixels in the*STEREO*/HI-1A). Both these stars are of spectral type F0; however, the eclipses include a substantial amount of time in the ingress and egress phases. The eclipses are consistently about 30 mmag deep and 2.2604 d apart. This is a transit by a larger, stellar body rather than a brown dwarf but a low-mass star remains a possibility.

The star HD 222891 has similar features to HIP 248; however, the eclipses are also too deep, at 40 mmag, with the host star of spectral type F8, to be due to a brown dwarf companion. It may nevertheless be a low-mass star of some interest.

Of all eclipse-like features extracted from the *STEREO*/HI-1A data base, the shallowest primary eclipses were 7 mmag deep around the star 18 Sgr. This light curve appears more like a contact binary, although the raw light curve is also somewhat irregular and the behaviour might instead be due to rotational microvariability. It was not considered conclusive enough to be labelled as an EB and does not feature in the sample, although more data may help to clarify the light curve and its classification.

NSV 1321 is the most marginal detection in the sample. In order to verify whether the 10-mmag eclipses observed were genuine, differential photometry was carried out; however, this appeared to introduce variability from a neighbouring star – it is located in a crowded field with several stars showing clear variability and others blended. Although the star itself is classified as a variable, the NSV catalogue as shown in the SIMBAD indicates that this variability was considered doubtful by the catalogue's compilers. With the host star of spectral type B8V, this would not be an exoplanet signal and is most likely a grazing eclipse or stellar companion. Although the possibility of microvariability or a blend with a neighbouring star cannot be completely ruled out, none of the neighbouring stars shows a periodicity of 2.2663 d, so this was included in the sample.

Another star showing shallow eclipses that was ruled out from being a brown dwarf is II Cnc (period from the *STEREO*/HI-1A of 1.0684 d, eclipses 25 mmag deep). This is listed in the SIMBAD as a BY Draconis type variable of spectral type G8V; however, there is no mention of it showing eclipses. The shape of the light curve is indicative of either a contact binary or grazing stellar transits with secondary eclipses present. The period is more representative of a contact binary. The secondary may nevertheless be a low-mass star, making this a relatively unusual system for a contact binary.

5 SURVEY PROSPECTS

Although the analysis thus far done has been restricted to recovering EBs and searching for exoplanets, the prospects for recovering variables of different types have been investigated.

The prospects for exoplanet extraction are summarized in Fig. 29 for the declination strips away from the Galactic plane for the ranges of periods and magnitudes shown. This indicates reasonable prospects for finding a signal, if any exists around stars of about 7th magnitude or brighter but with a sharp fall-off for fainter stars, such that the probability of extraction is negligible for stars fainter than 8th magnitude from *STEREO*/HI-1A data alone. Note that the most significant substellar candidate so far extracted is magnitude 7.5. For reference, the signal of HIP 247 and HIP 248 (magnitude 7.5, period 2.2604 d) is 30 mmag deep detected with a significance of 5σ and the 30 mmag deep signal of HR 1750 (magnitude 6.5, period 3.3150 d) is detected with a significance of 8σ. With the inclusion of *STEREO*/HI-1B data, the number of data points will more than double (this satellite is in an Earth-trailing orbit and stars

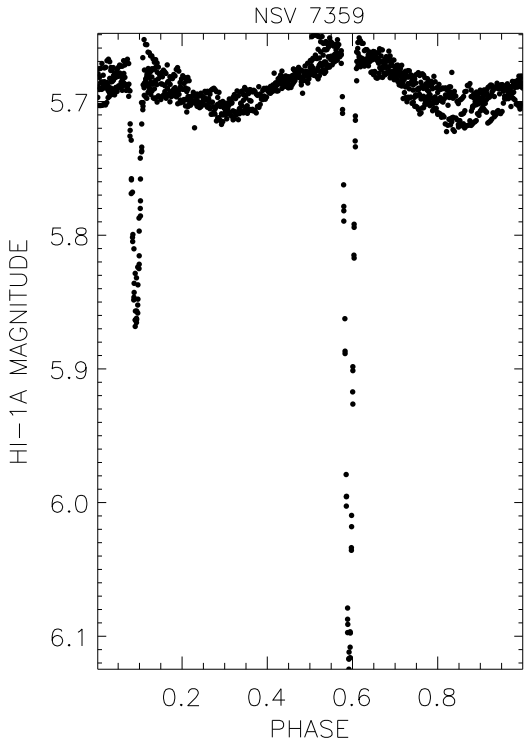

Figure 26. Light curve of the star NSV 7359, phase-folded on a period of 9.1999 d.

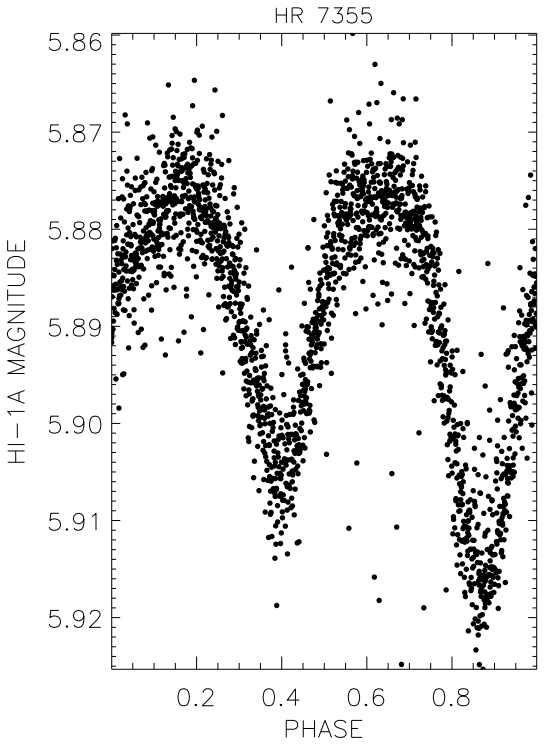

Figure 27. Light curve of the star HR 7355, phase-folded on a period of 0.5214 d.

remain in the field of view for longer) and the significance of extracted signals will increase, as will the potential for extracting faint signals.

For EBs, Figs 14, 17 and 28 indicate that more may yet be found and Fig. 11 shows that the combination of the BLS and Lomb–Scargle methods is a good way of extracting their signals. The difficulty here is that, from photometric data alone, it has not been possible to conclusively classify them as EBs. This problem largely affects contact binaries, which have light curves that might easily be confused with elliptical variables and short-period pulsating stars. The ability of the Lomb–Scargle method to extract contact binaries suggests it would be a useful tool for extracting other variables also.

Asteroseismological studies are likely to require that low-level variability be detected. If a signal of 10 mmag, comparable to an exoplanet transit, is required, then Fig. 29 might also be an indicator of the prospects for extracting microvariable behaviour; however, this would assume that the algorithm chosen to extract the microvariable signal is equally effective at discerning faint signals as the BLS. Nevertheless, the prospects would appear good for the brighter stars (7th magnitude or brighter) and these are also the most amenable to high-resolution spectroscopic follow-up by other observatories. Investigations of the signals extracted by the Lomb–Scargle method show that the presence of systematic sources of noise inhibits the detection of a test signal, however, so additional cleaning would be required. Whilst the observing cadence of 40 min will impair detailed studies of very short period variables, the ongoing examination of the data that is including *STEREO*/HI-1B observations is nevertheless able to obtain very clear photometry from a number of known δ Scuti stars (e.g. DX Cet) and potentially detect new variables down to magnitude 11.

6 CONCLUSIONS

The *STEREO*/HI-1A observations are clearly a valuable resource suitable for a wide range of variability studies. With 263 EBs extracted from the data base, 122 of which have not previously been identified as such, there is the potential for the discovery of a number of new and interesting objects. The area of the sky being covered and the brightness of the stars being observed are features unique to the *STEREO*/HI-1A and simultaneously allow for high-quality follow-up observations of interesting objects. There is the potential to discover transiting exoplanets (Fig. 29); however, this is at the very limit of the survey's sensitivity and would only be possible for the stars with the cleanest signals. A 30-mmag transit around a magnitude 7.5 star is detectable with 5σ significance and a 30-mmag transit of a magnitude 6.5 star is detectable with 8σ significance from *STEREO*/HI-1A data alone. With the inclusion of data from the second satellite, the *STEREO*/HI-1B, this will improve; for example, from *STEREO*/HI-1A data alone the 50-mmag transits of the magnitude 8.5 star BD +03 263p are detected with 7σ significance, but with the inclusion of *STEREO*/HI-1B data, they are detected with nearly 13σ significance.

The analysis presented here may have some impact on stellar evolution studies, in particular relating to the proportion and distribution of eccentric EBs. As the newly discovered EBs are comparatively bright, the masses, radii and effective temperatures can be determined more accurately in follow-up observations and can therefore provide more stringent tests of stellar evolution models (e.g. Claret & Willems 2002; Stassun et al. 2006; Torres et al. 2006; VandenBerg et al. 2006). The new EBs will also help to produce more accurate distances to their host stars and any stars those are associated with (Southworth, Maxted & Smalley 2005).

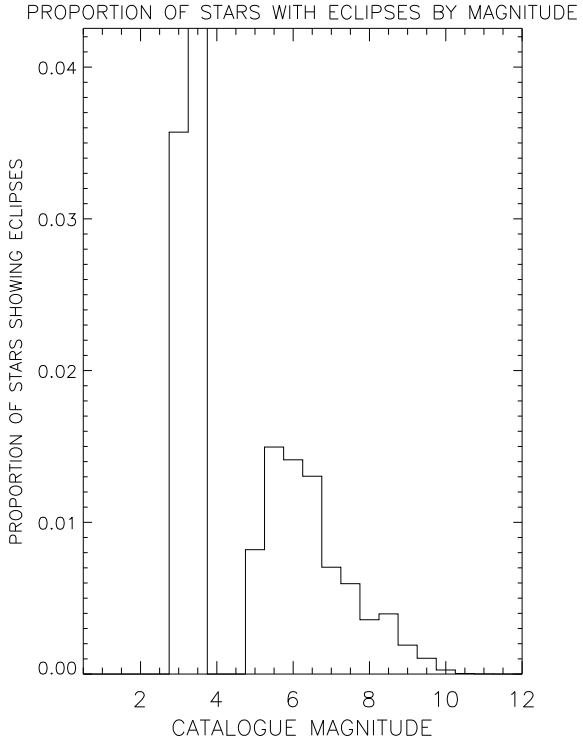

Figure 28. The proportion of stars of different magnitudes that have been found to be eclipsing. The small number of stars brighter than magnitude 4.5 in the *STEREO*/HI-1A field of view is responsible for the shape at the bright end of this graph, with only three EBs observed.

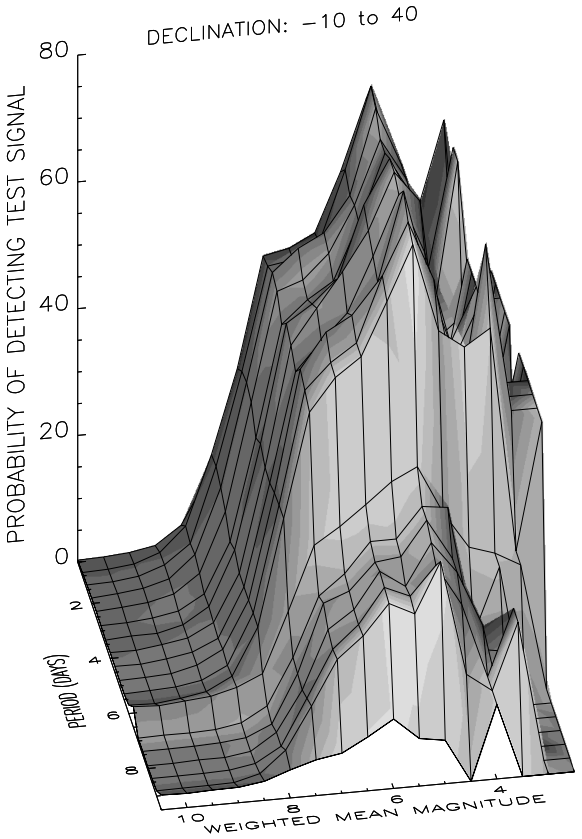

Figure 29. The percentage of stars where a 10-mmag test eclipse superimposed on the real light curve was successfully returned as the strongest signal by the BLS algorithm. Each epoch of each star was examined separately and only those that returned the test signal within 0.04 d were considered successes. Detection of a harmonic was not considered a success. This graph thus represents the chance of detecting a transiting 'Hot Jupiter' for stars of a given magnitude for the range of periods shown. The stars tested were those with a declination between -10° and 40° and having a weighted mean magnitude within 0.05 mag of the points shown. The trial periods ranged from 0.5 to 9.5 d in half-day steps. The dip in success rates at 6.5 d is the result of many stars having parts of their light curve masked out to avoid the contamination by solar activity, whilst the dip at 9.5 d is the result of fewer stars remaining in the field of view for long enough for a period of this length to be checked. The small increases in success rates for fainter stars at these periods are due to artificial trends associated with the length of an epoch, which also contributes to an increase in the number of false positives for brighter stars, although this number is small compared to the decreases observed for the above reasons. The best substellar candidate so far extracted has a period of 2.4238 d and a host star of magnitude 7.5: a 25-mmag transit is detectable with 5σ significance at this level.

The potential to improve upon the existing phase coverage, especially relating to that obtained during eclipses, and times of maxima and minima in a variability cycle can help to refine parameters for these important stars. In some cases, the capability of the *STEREO* to deliver good photometry over time-scales of days and weeks in a single pass, combined with repeated observations after about a year, is ideal for observing long-term changes in variability. This is of particular importance in studies of magnetic activity cycles (eg. V471 Tau) and particular classes of variables, such as RS CVn stars (eg. SZ Psc).

The EBs newly discovered by this analysis show a tendency to possess shallower transits than those previously known (Fig. 18), partly due to the quality and cadence of the photometry. With many of the host stars being of early spectral types, late B and early A, it is possible that many of these systems may be comparatively young (Fig. 8). A small but significant proportion are in eccentric orbits (Figs 6 and 7), supporting recent observations by *Kepler* (Prša et al. 2011). Some particularly interesting systems have been identified for potential follow-up observations, including one good brown dwarf candidate (HD 213597, Fig. 20). The proportion of stars of different magnitudes found to be eclipsing indicates that more may yet be found as Fig. 28 shows decreasing numbers observed with fainter stars, whereas the real number should be a constant proportion of the population.

Evaluation of the algorithms used to extract EBs suggests that, if exoplanets alone are the target, then the BLS algorithm is capable of effectively extracting them (Fig. 29). For a more general search for EBs, however, the combination of the BLS and Lomb–Scargle periodogram analyses will be required in order to extract a high proportion of these objects (Fig. 11). The Stetson index can be used as a measure of noise, as well as variability, although it does rate some Algol-type binaries very highly, so extreme values are not necessarily false positives (Fig. 14).

Further research being done includes the development of a matched filter algorithm and follow-up observations of key targets have been started to be made. A further two EBs showing eccentricity have been discovered (TYC 1422-1328-1, magnitude in the *STEREO*/HI-1A of 9.5, period 3.0999 d, $|e \times \cos\omega| = 0.175 \pm 0.025$ with the primary and secondary eclipses both 0.1 mag deep, and BD +09 485, magnitude in the*STEREO*/HI-1A of 9.15, period 4.5293 d, $|e \times \cos\omega| = 0.125 \pm 0.025$ with the primary eclipses 0.15 mag deep and secondary eclipses 0.1 mag

deep), amongst numerous other short-period variables. Periods have been extracted for a variety of stars showing sinusoidal-like variations in their light curve and some stars showing changes in behaviour on a year-by-year basis have been observed (e.g. V 471 Tau, SZ Psc). Additional findings will be reported in due course.

ACKNOWLEDGMENTS

The HI instrument was developed by a collaboration that included the Rutherford Appleton Laboratory and the University of Birmingham, both in the United Kingdom, the Centre Spatial de Liège (CSL), Belgium, and the US Naval Research Laboratory (NRL), Washington DC, USA. The *STEREO*/SECCHI project is an international consortium of the NRL (USA), Lockheed Martin Solar and Astrophysics Lab (USA), NASA Goddard Space Flight Center (USA), Rutherford Appleton Laboratory (UK), University of Birmingham (UK), Max-Planck-Institut für Sonnensystemforschung (Germany), Centre Spatial de Liège (Belgium), Institut d'Optique Théorique et Appliquée (France) and Institut d'Astrophysique Spatiale (France). This research has made use of the SIMBAD operated at CDS, Strasbourg, France, the NASA's Astrophysics Data System and the statistical analysis package R (R Development Core Team 2008). This research has also made use of the PERANSO (version 2.31) light-curve and period-analysis software maintained at CBA, Belgium Observatory (http://www.cbabelgium.com). This research is funded by the Science and Technology Facilities Council. This research has also made use of an IDL program to carry out a Lomb–Scargle periodogram analysis, from the Armagh Observatory at http://www.arm.ac.uk/ csj/idl/PRIMITIVE/scargle.pro. KTW acknowledges support from an STFC studentship. Many thanks to the referee for numerous thoughtful and constructive comments that have improved the quality of the paper.

REFERENCES

Auvergne M. et al., 2009, A&A, 506, 411
Bewsher D., Brown D. S., Eyles C. J., Kellett B. J., White G. J., Swinyard B., 2010, Sol. Phys., 264, 1
Brown D. S., Bewsher D., Eyles C. J., 2009, Sol. Phys., 254, 185
Claret A., Willems B., 2002, A&A, 388, 518
de Mink S. E., Langer N., Izzard R. G., 2011, Bull. Soc. R. Sci. Liège, 80, 543
Eyles C. J. et al., 2009, Sol. Phys., 254, 387
Hussain G., Allende Prieto C., Saar S., Still M., 2006, MNRAS, 367, 1699
Kaiser M. L., Kucera T. A., Davila J. M., St. Cyr O. C., Guhathakurta M., Christian E., 2008, Space Sci. Rev., 136, 5
Kamiński K. et al., 2007, AJ, 134, 1206
Koch D. G. et al., 2010, ApJ, 713, L79
Kovács G., Zucker S., Mazeh T., 2002, A&A, 391, 369
Kozai Y., 1962, AJ, 67, 591
Mathieu R. D., Mazeh T., 1988, AJ, 326, 256
O'Brien M., Bond H., Sion E., 2001, ApJ, 563, 971
Oksala M. E., Wade G. A., Marcolino W. L. F., Grunhut J., Bohlender D. A., Manset N., Townsend R. H. D., the MiMeS Collaboration, 2010, MNRAS, 405, L51
Pollacco D. L. et al., 2006, PASP, 118, 1407
Prša A. et al., 2011, AJ, 141, 83
R Development Core Team, 2008, R: A Language and Environment for Statistical Computing. R Foundation for Statistical Computing, Vienna, Austria
Scargle J. D., 1982, ApJ, 263, 835
Southworth J., Maxted P. F. L., Smalley B., 2005, A&A, 429, 645
Stassun K. G., Mathieu R. D., Valenti J. A., 2006, Nat, 440, 311
Torres G., Lacy C. H., Marschall L. A., Sheets H. A., Mader J. A., 2006, ApJ, 640, 1018
VandenBerg D. A., Bergbusch P. A., Dowler P. D., 2006, ApJS, 162, 375
Vanmunster T., 2008, Peranso Light Curve and Period Analysis Software. CBA Belgium Observatory, Landen
Welch D. L., Stetson P. B., 1993, AJ, 105, 1813
Zacharias N., Monet D., Levine S., Urban S., Gaume R., Wycoff G., 2004, BAAS, 36, 1418

APPENDIX A: ECCENTRIC ECLIPSING BINARIES

Fig. A1 outlines the data reduction pipeline. The measurably eccentric EBs are shown in Fig. A2, along with the light curve of HD 173770, which, although not included in the sample owing to an inability to uniquely determine its period due to the small number of eclipses observed, nevertheless appears to be an eccentric EB. The $|e \times \cos\omega|$ measured for this star is 0.108 ± 0.012 and the light curve shown is a phase-folding on a period of 25.145 d. The values of $|e \times \cos\omega|$ measured for the other stars can be found in Table A1 (only a sample is shown here; the full table is available with the online version of the article – see Supporting Information). The identities of the stars are as given in the table; however, in the cases where nearby stars may have contaminated the signal or be the real source of eclipses, it was often the case that the eclipses would feature in multiple light curves and the ones selected for the analysis were those that were clearer and had deeper eclipses and higher SDE. Where this occurred, the table gives the name of a star that may be contaminating the light curve or be the real source of eclipses.

In Table A1, where data are not available, for example, because secondary eclipses were not visible or the spectral type has yet to be determined, the entry is given as NA. The right ascension and declination are given in degrees. The primary eclipse depth and weighted mean magnitude are both in units of magnitudes. Periods are in units of days. The BLS SDE, the peak power from a Lomb–Scargle periodogram analysis and the Stetson variability index are all arbitrary scalar units. The estimates of the minimum eccentricity ($|e \times \cos\omega|$) and the estimated errors in those estimates are all scalar values. The spectral type given is for the closest star to the listed coordinates from the SIMBAD, the identity of which is given in the next column. The alternative nearby star is the identity of a nearby star that might be the source of the eclipses, rather than the closest star (this frequently occurs due to the 70 arcsec pixel^{-1} resolution of the *STEREO*/HI-1A, as well as being due to nearby bright EBs). The known EB is a binary flag set to 1 if either star is recorded as showing eclipses and 0 otherwise.

APPENDIX B: LIGHT CURVES

The light curves for all EBs in the sample, including HD 173770, are given with the online version of the article as Figs B1–B11 (see Supporting Information).

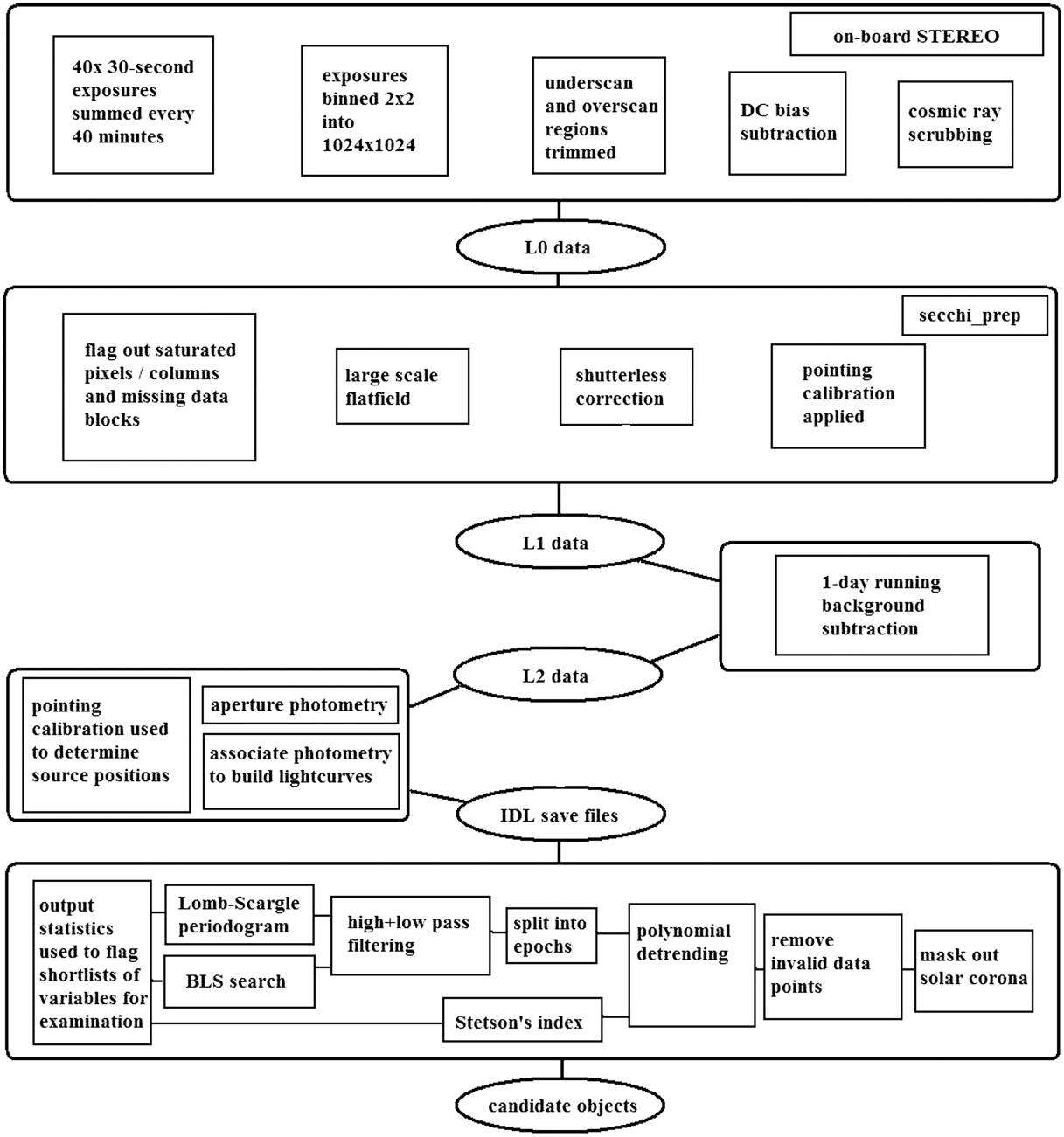

Figure A1. The *STEREO*/HI-1A data analysis pipeline.

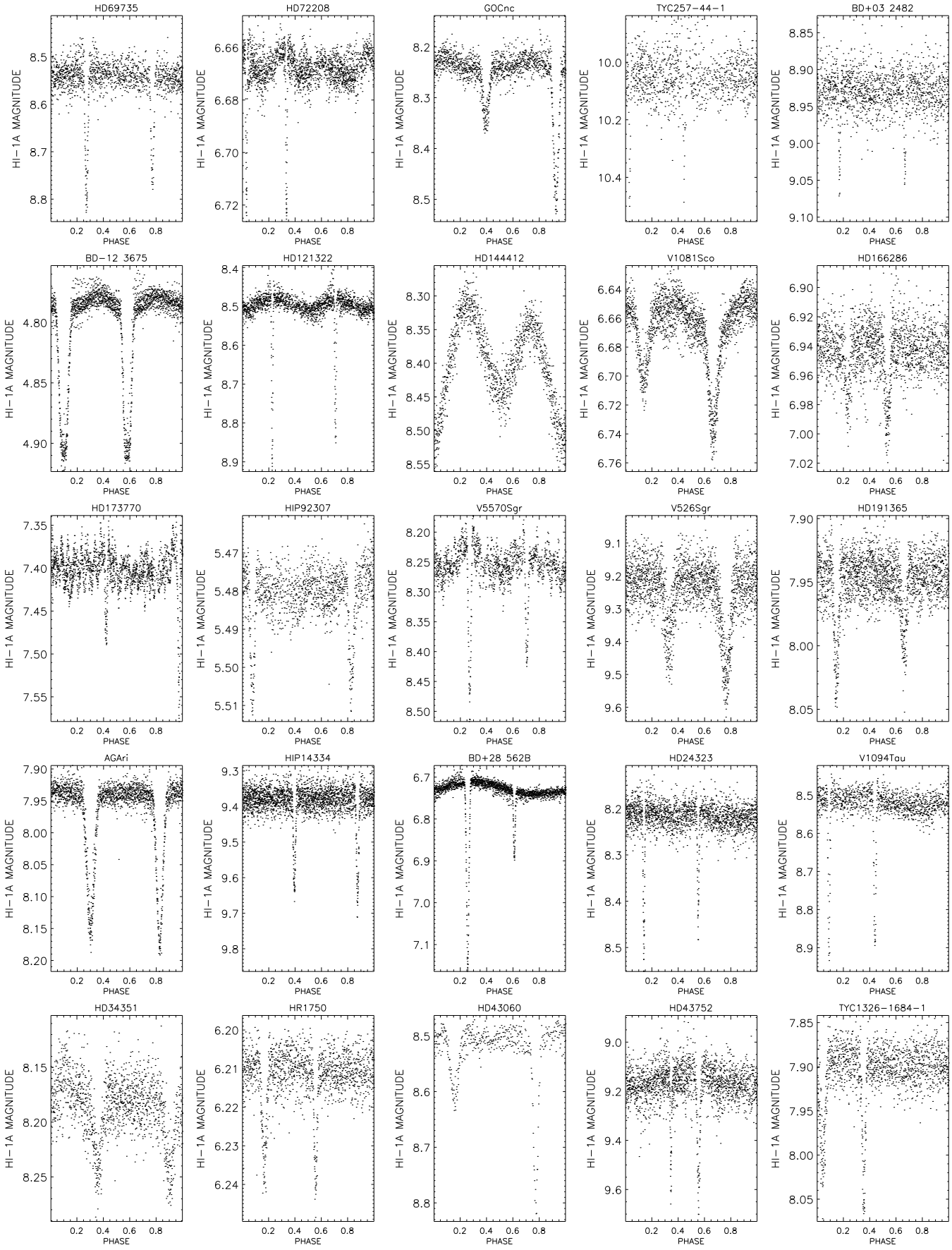

Figure A2. Light curves of all measurably eccentric EBs in the sample and the best-fitting light curve of HD 173770 (see Section 4).

Table A1. 263 EBs found from *STEREO*/HI-1A data. Only a sample is shown here – the full table is available with the online version of the article (see Supporting Information).

RA	Dec.	Primary eclipse depth	Period	Weighted mean magnitude	BLS SDE	Stetson index	Peak Lomb–Scargle power	$\|e \times \cos\omega\|$	$\pm$ error in $\|e \times \cos\omega\|$	Spectral type	Identity	Alternative nearby star	Known EB
58.306	30.1915	0.15	0.791 65	9.6355	4.985	0.089 959	163.27	0.014	0.05	A0	HD 281317	NA	0
99.8127	31.5917	0.06	4.763	8.1252	4.0087	0.095 906	83.309	NA	NA	F5	HD 261026	AK Aur	1
92.5473	30.0289	0.15	0.9815	8.7237	4.9764	0.108 18	111.68	0.002	0.02	A0	V 576 Aur	NA	1
94.4646	32.5046	0.07	2.7361	7.0957	5.7669	0.121 52	102.39	0.008	0.024	A3	V 406 Aur	NA	1
98.1133	32.4549	0.55	2.5250	5.7419	6.1559	95.241	101.2	0.03	0.04	A3m	WW Aur	NA	1
98.9069	32.5768	0.4	1.065	7.7216	4.163	4.0988	272.15	0.00	0.036	B8	V 459 Aur	NA	1
101.605	31.4128	0.13	4.6835	8.6636	3.1958	0.109 23	189.26	0.025	0.07	G5	HD 263268	HD 263212	0
33.8366	22.5697	0.2	1.027 75	8.3924	5.9916	1.1283	133.77	0.01	0.03	F2V	RX Ari	NA	1
37.7781	22.1983	0.25	0.3963	9.1747	3.7634	0.1098	294.49	0.00	0.06	F8	BD +21 345	NA	0
50.8846	25.8994	0.1	1.305 55	9.2946	8.3623	0.034 856	81.708	NA	NA	F5	BD +25 539	NA	0
52.3671	21.1134	0.2	4.989 75	9.1	4.5718	0.1323	40.661	NA	NA	F2	CCDM J03295+2107AB	NA	0
52.2775	27.4136	0.4	1.0	9.2641	4.1739	0.591 02	268.03	0.01	0.036	F2	BD +26 560	NA	1
55.0698	26.8486	0.12	6.114	7.4839	6.2441	0.075 213	53.906	0.00	0.02	B9	BD +26 597	NA	0
55.1605	28.7716	0.45	8.1665	6.7556	7.38	3.8155	34.838	0.294	0.006	A2V	BD +28 562B	HD 22766	1
57.0867	23.4213	0.01	2.2663	5.3929	2.764	0.001 3492	227.86	NA	NA	B8V	NSV 1321	NA	0
57.8397	25.6354	0.15	0.631 45	8.4441	4.8421	0.073 541	138.34	NA	NA	G5	HD 24105	NA	0
58.2809	25.5354	0.3	6.530 65	8.2552	4.8853	0.213 81	35.026	0.18	0.006	A0	HD 24323	SX Tau	1
59.0473	29.523	0.7	1.6144	10.2486	6.14114	0.258 88	172.29	0.01	0.06	A3	AN Tau	NA	1
69.5660	20.6847	0.75	2.0555	5.8251	7.189	100.44	69.73	0.01	0.03	B8V	HU Tau	NA	1
60.9763	28.126	2.3	2.7778	7.9245	6.5421	35.085	73.255	0.00	0.035	B8Ve	RW Tau	NA	1
61.8078	29.309	1.2	5.3604	10.9617	6.4905	0.327	63.897	NA	NA	NA	IL Tau	NA	1
63.015	21.9474	0.4	9.0	8.5775	4.4708	0.217 27	25.498	0.305	0.02	G0	V1094 Tau	NA	1
69.7778	22.7121	0.1	0.7641	8.3943	4.2479	0.053 07	166.57	NA	NA	B5	HD 284583	NA	0
73.9828	27.8354	0.06	1.2222	8.1691	4.9429	0.022 643	109.84	0.005	0.04	F8	HD 31328	AQ Tau	1
74.7198	24.4957	0.38	0.6944	7.6702	4.8047	24.254	199.61	NA	NA	B5	V1061 Tau	NA	1
76.4072	23.0611	0.23	1.7778	6.5015	4.9423	1.9962	96.445	0.02	0.02	B5	V1154 Tau	NA	1
79.3798	20.1318	0.5	1.717 55	6.3583	6.5897	13.857	51.274	NA	NA	F7V	CD Tau	NA	1
79.4109	20.5354	0.07	2.6419	8.2016	3.5365	0.015 735	120.34	0.095	0.04	B9	HD 34351	NA	0

SUPPORTING INFORMATION

Additional Supporting Information may be found in the online version of this article:

Table A1. 263 EBs found from *STEREO*/HI-1A data.
Figures B1–B11. Light curves of all EBs in the sample including HD 173770 (see Section 4).

Please note: Wiley-Blackwell are not responsible for the content or functionality of any supporting materials supplied by the authors. Any queries (other than missing material) should be directed to the corresponding author for the article.

This paper has been typeset from a TEX/LATEX file prepared by the author.